Peiman Naseradinmousavi
Assistant Professor
Dynamic Systems and
Control Laboratory (DSCL),
Department of Mechanical Engineering,
San Diego State University,
San Diego, CA 92115
e-mails: pnaseradinmousavi@mail.sdsu.edu;
peiman.n.mousavi@gmail.com

Hashem Ashrafiuon
Professor
Director of Center for
Nonlinear Dynamics and Control,
Department of Mechanical Engineering,
Villanova University,
Villanova, PA 19085
e-mail: hashem.ashrafiuon@villanova.edu

Mohammad A. Ayoubi
Department of Mechanical Engineering,
Santa Clara University,
Santa Clara, CA 95053
e-mail: maayoubi@scu.edu

An Adaptive Centralized Approach to Control Chaotic and Hyperchaotic Dynamics of Smart Valves Network

Catastrophic chaotic and hyperchaotic dynamical behaviors have been experimentally observed in the so-called "smart valves" network, given certain critical parameters and initial conditions. The centralized network-based control of these coupled systems may effectively mitigate the harmful dynamics of the valve-actuator configuration which can be potentially caused by a remote set and would gradually affect the whole network. In this work, we address the centralized control of two bi-directional solenoid actuated butterfly valves dynamically coupled in series subject to the chaotic and hyperchaotic dynamics. An interconnected adaptive scheme is developed and examined to vanish both the chaotic and hyperchaotic dynamics and return the coupled network to its safe domain of operation. [DOI: 10.1115/1.4037593]

1 Introduction

Dangerous dynamical behaviors of multidisciplinary systems, in particular the electromechanical ones, need to be controlled in order to avoid the expected failure of the large-scale network. The so-called smart valves network, containing many interconnected electro-magneto-mechanical-fluid components, plays an important role in proper and efficient performance of many critical infrastructures which include, but are not limited to, municipal piping systems, oil and gas fields, petrochemical plants, and the U.S. Navy. The latter utilizes a distributed flow control system for cooling purposes, and therefore, the failure of such a crucial unit would expectedly impose considerable costs of restoration and operation. A robust control scheme is, hence, required to mitigate the effects of the harmful dynamic responses in the presence of uncertainties involved with such a large-scale network.

We have reported broad analytical and experimental studies [1–13] for both an isolated actuator-valve arrangement and a network of two interconnected solenoid actuated butterfly valves operating in series. A novel third-order nondimensional analytical model of the single solenoid actuated butterfly valve was derived dealing with the coupled nonlinear magnetic, hydrodynamic, and bearing torques [8]. We then could capture transient chaotic and crisis dynamics of the isolated set [6,13] by exposing the actuator-valve system to the critical values of nondimensional magnetic force's coefficient and equivalent viscous damping. Such a nonlinear analysis led us to determine the bounds needed to operate the system within a safe domain. These bounds helped us optimize the isolated set design and then operation by yielding upward of 40% energy savings [5].

The isolated analysis could expectedly provide an insightful practice to thoroughly understand the undergoing physics of the system. Although the results of such an analysis could be improved considering the interconnections among the neighbor sets, we have developed a nonlinear coupled model of two actuator-valve sets operating in series without the pipe contraction [4]. A periodic noise was intentionally applied on the upstream valve to examine its effects on the downstream set of valve-actuator. A powerful tool of the nonlinear analysis, the power spectrum, was used in revealing the same oscillation frequency of the downstream set with that of the upstream one but with smaller amplitudes. We have also reported the nonlinear analytical model of two interconnected sets subject to the pipe contraction in Refs. [1,2,9,12].

The coupled design optimization was then carried out for the interconnected sets using global optimization tools [2,11,12], which yielded upward of 13% energy savings. A constrained optimization problem was solved with respect to the parameters' bounds determined through the nonlinear dynamic analysis [1,3]. We, for the first time, captured chaotic and hyperchaotic dynamics of the coupled sets for some critical parameters and initial conditions. Some powerful tools of the nonlinear analysis, including the Lyapunov exponents and Poincaré map, were utilized in characterizing the responses coupled in various aspects. One and two positive Lyapunov exponents confirmed the chaotic and hyperchaotic dynamics of the network of actuators-valves, respectively. We have also presented bifurcation diagrams to reveal the transition from the chaotic dynamics to the hyperchaotic one. A larger domain of attraction was expectedly revealed for the hyperchaotic response than the chaotic one.

The coupled operational optimization was another important phase which we have carried out [3] to minimize the lumped energy consumption. The stability analysis reported in Ref. [1] yielded the safe domain of operation. The safe domain of operation helped us carry out a constrained operational optimization by fitting nonlinear trajectories to the valves' stable motions. The coefficients of the trajectories fitted were then optimized examining four global optimization schemes to avoid being trapped in several possible local minima. The local and global design sensitivity analyses were also performed to examine the sensitivity of the cost function defined to the optimization variables. The step size analysis yielded an optimal step size to significantly reduce both the computational cost (iteration) and time. The effects of the pipe contraction angle (approach angle) on the amount of energy saved were then studied. We concluded that the smaller approach angle yields a higher lumped amount of energy saving.

Finding specific research work to capture and control the chaotic and hyperchaotic dynamics of such a multiphysics network is somewhat difficult, although some efforts have been reported for similar case studies. Chang-Jian [14] have studied gear dynamics with turbulent journal bearings mounted hybrid squeeze film

Contributed by the Design Engineering Division of ASME for publication in the Journal of Computational and Nonlinear Dynamics. Manuscript received October 25, 2016; final manuscript received July 29, 2017; published online October 9, 2017. Assoc. Editor: Hiroshi Yabuno.

damper. In order to avoid the nonsynchronous chaotic vibrations, they utilized an increased proportional gain $K_p = 0.1$ to control this system. It was shown that the pinion trajectory will leave chaotic motion to periodic motion in the steady state under control action. Morel et al. [15] proposed a new nonlinear feedback, which induces chaos and which was able at the same time to achieve a low spectral emission and to maintain a small ripple in the output. The design of this new and simple controller was based on the propriety that chaotified nonlinear systems present many independent chaotic attractors of small dimensions. Chen and Liu [16] investigated chaos control of fractional-order energy demand-supply system by two different control strategies: a linear feedback control and an adaptive switching control strategy via a single control input. Some other efforts related to the chaos control can be found in Refs. [17–28].

The last phase of this research effort is nonlinear control of the network subject to the chaotic and hyperchaotic dynamics which we have previously captured. We here briefly represent the interconnected analytical model of two sets (for completeness) along with the critical initial conditions and parameters resulted in the dangerous responses. The coupled adaptation and control laws will be formulated with respect to the interconnected dynamics of the system. The results will be thoroughly discussed to address the robustness of adaptive scheme for vanishing the chaotic and hyperchaotic dynamics.

2 Mathematical Modeling

The system, which is being considered here, is two bi-directional solenoid actuated butterfly valves operating in series. The system undergoes a sudden pipe contraction as shown in Fig. 1. The plungers are connected to the valves' stems through the rack and pinion arrangements yielding kinematic constraints.

We have previously derived the interconnected analytical model of two sets operating in series [1,2,9,12] and briefly represent here for completeness. Some simplifying assumptions have been made to develop the analytical formulas of the coupled sets. The first one is to assume a negligible magnetic "diffusion time" with respect to a nominal operation time (40 s). Note that the diffusion time has an inverse relationship with the amount of current applied. The second assumption is the existence of laminar flow. We have carried out experimental work for an isolated set to validate the assumption of laminar flow. The total flow loads, including hydrodynamic (T_h) and bearing (T_b) torques, were measured experimentally for the inlet velocity of $v \approx 2.7\,\text{m/s}$ and valve diameter of $D_v = 2$ in to be compared with the analytical formulas. An acceptable consistency was observed between the analytical and experimental approaches [29].

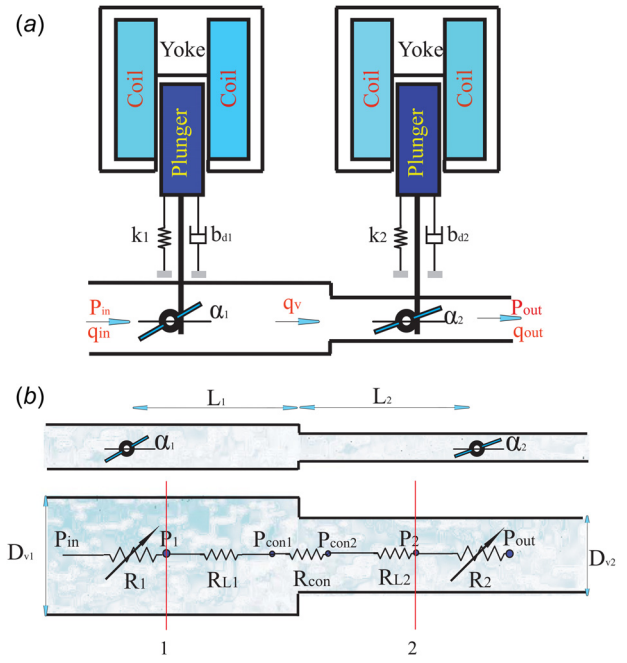

Fig. 1 (*a*) A schematic configuration of two bi-directional solenoid actuated butterfly valves subject to the sudden contraction and (*b*) a coupled model of two butterfly valves in series without actuation

As can be observed in Fig. 1(*b*), the valves are modeled as changing resistors

$$R_{n1}(\alpha_1) = \frac{e_1}{\left(p_1\alpha_1^3 + q_1\alpha_1^2 + o_1\alpha_1 + \gamma_1\right)^2} \tag{1}$$

$$R_{n2}(\alpha_2) = \frac{e_2}{\left(p_2\alpha_2^3 + q_2\alpha_2^2 + o_2\alpha_2 + \gamma_2\right)^2} \tag{2}$$

where R_{n1} and R_{n2} indicate the resistances of the upstream and downstream valves, respectively, and $e_1 = 7.2 \times 10^5, p_1 = 461.9$, $q_1 = -405.4$, $o_1 = -1831$, $\gamma_1 = 2207$, $e_2 = 4.51 \times 10^5$, $p_2 = 161.84, q_2 = -110.53$, $o_2 = -695.1$, and $\gamma_2 = 807.57$ for two different valves' diameters. Also the flow between the valves in addition to the sudden contraction are modeled as constant resistors based on the Hagen–Poiseuille and Borda–Carnot formulas [30,31]

$$R_{L1} = \frac{128\mu_f L_1}{\pi D_{v1}^4} \tag{3}$$

$$R_{L2} = \frac{128\mu_f L_2}{\pi D_{v2}^4} \tag{4}$$

$$R_{\text{con}} = \frac{8K_{\text{con}}}{\pi^2 D_{v2}^4} \tag{5}$$

where $K_{\text{con}} = 0.5(1-\beta^2)\sqrt{\sin(\theta/2)}$, β indicates the ratio of minor and major diameters (D_{v2}/D_{v1}), θ is the angle of approach (the pipe contraction angle), μ_f stands for the fluid dynamic viscosity, D_{v1} and D_{v2} are the upstream and downstream valves' diameters, respectively, L_1 and L_2 indicate the pipe lengths before and after contraction, and R_{L1} and R_{L2} are the constant resistances. Therefore, two valves operating in series can be modeled as a set of five resistors leading us to derive mathematical expressions of the pressures after and before the upstream and downstream valves, respectively, as follows [1,2,9,12]:

$$P_1 = \frac{R_{n2}P_{\text{in}} + R_{n1}P_{\text{out}} + R_{n1}(R_{L1} + R_{L2} + R_{\text{con}}q_v)q_v}{(R_{n1} + R_{n2})} \tag{6}$$

$$P_2 = \frac{R_{n2}P_{\text{in}} + R_{n1}P_{\text{out}} - R_{n2}(R_{L1} + R_{L2} + R_{\text{con}}q_v)q_v}{(R_{n1} + R_{n2})} \tag{7}$$

where q_v is the volumetric flow rate. These interconnected pressures were used in developing both the coupled hydrodynamic and bearing torques [1,2,9,12]

$$\begin{aligned} T_{h1} &= \left(a_1\alpha_1 e^{b_1\alpha_1^{1.1}} - c_1 e^{d_1\alpha_1}\right)(P_{\text{in}} - P_1) \\ &= \left(a_1\alpha_1 e^{b_1\alpha_1^{1.1}} - c_1 e^{d_1\alpha_1}\right) \times \frac{\dfrac{e_1}{\left(p_1\alpha_1^3 + q_1\alpha_1^2 + o_1\alpha_1 + \gamma_1\right)^2}}{\displaystyle\sum_{i=1}^{2} \frac{e_i}{\left(p_i\alpha_i^3 + q_i\alpha_i^2 + o_i\alpha_i + \gamma_i\right)^2}} \\ &\quad \times \left(P_{\text{in}} - P_{\text{out}} - (R_{L1} + R_{L2} + R_{\text{con}}q_v)q_v\right) \end{aligned} \tag{8}$$

$$T_{h2} = \left(a_1'\alpha_2 e^{b_1'\alpha_2^{1.1}} - c_1' e^{d_1'\alpha_2}\right)(P_2 - P_{\text{out}})$$
$$= \left(a_1'\alpha_2 e^{b_1'\alpha_2^{1.1}} - c_1' e^{d_1'\alpha_2}\right) \times \frac{\dfrac{e_2}{\left(p_2\alpha_2^3 + q_2\alpha_2^2 + o_2\alpha_2 + \gamma_2\right)^2}}{\displaystyle\sum_{i=1}^{2} \frac{e_i}{\left(p_i\alpha_i^3 + q_i\alpha_i^2 + o_i\alpha_i + \gamma_i\right)^2}}$$
$$\times \left(P_{\text{in}} - P_{\text{out}} - (R_{L1} + R_{L2} + R_{\text{con}}q_v)q_v\right) \tag{9}$$

$$T_{b1} = C_1 \Delta P_1(R_{n1}, R_{n2}, R_{L1}, R_{L2}, R_{\text{con}}) \tag{10}$$

$$T_{b2} = C_2 \Delta P_2(R_{n1}, R_{n2}, R_{L1}, R_{L2}, R_{\text{con}}) \tag{11}$$

where $a_1 = 0.4249$, $a_1' = 0.1022$, $b_1 = -18.52$, $b_1' = -17.0795$, $c_1 = -7.823 \times 10^{-4}$, $c_1' = -2 \times 10^{-4}$, $d_1 = -1.084$, $d_1' = -1.0973$, $C_1 = C_2 = 0.5 A_d \mu D_s$, $\Delta P_1 = P_{\text{in}} - P_1$, $\Delta P_2 = P_2 - P_{\text{out}}$, and P_{in} and P_{out} are the given inlet and outlet pressures, respectively. Note that D_s is the stem diameter of the valve and μ stands for the friction coefficient of the bearing area. We have previously established that the hydrodynamic torque acts as a helping load pushing the valve to be closed and is typically effective for when the valve angle is lower than 60 deg [2,4]; the effective range was experimentally examined [4] confirming the helping behavior of the hydrodynamic torque by presenting positive values. The bearing torque, due to its friction-based nature, always acts as a resisting load.

Based on the analytical formulas addressed earlier, the sixth-order interconnected dynamic equations of two bi-directional solenoid actuated butterfly valves were developed as follows:

$$\dot{z}_1 = z_2 \tag{12}$$

$$\dot{z}_2 = \frac{1}{J_1}\left[\frac{r_1 C_{21} N_1^2 z_3^2}{2\left(C_{11} + C_{21}(g_{m1} - r_1 z_1)\right)^2} - b_{d1} z_2 - k_1 z_1 \right.$$
$$+ \frac{\dfrac{(P_{\text{in}} - P_{\text{out}} - (R_{L1} + R_{L2} + R_{\text{con}}q_v)q_v)e_1}{\left(p_1 z_1^3 + q_1 z_1^2 + o_1 z_1 + \gamma_1\right)^2}}{\sum_{i=1,4} \dfrac{e_i}{\left(p_i z_i^3 + q_i z_i^2 + o_i z_i + \gamma_i\right)^2}}$$
$$\left. \times \left[\left(a_1 z_1 e^{b_1 z_1^{1.1}} - c_1 e^{d_1 z_1}\right) - C_1 \times \tanh(K z_2)\right]\right] \tag{13}$$

$$\dot{z}_3 = \frac{(V_1 - R_1 z_3)\left(C_{11} + C_{21}(g_{m1} - r_1 z_1)\right)}{N_1^2}$$
$$- \frac{r_1 C_{21} z_3 z_2}{\left(C_{11} + C_{21}(g_{m1} - r_1 z_1)\right)} \tag{14}$$

$$\dot{z}_4 = z_5 \tag{15}$$

$$\dot{z}_5 = \frac{1}{J_2}\left[\frac{r_2 C_{22} N_2^2 z_6^2}{2\left(C_{12} + C_{22}(g_{m2} - r_2 z_4)\right)^2} - b_{d2} z_5 - k_2 z_4 \right.$$
$$+ \frac{\dfrac{(P_{\text{in}} - P_{\text{out}} - (R_{L1} + R_{L2} + R_{\text{con}}q_v)q_v)e_2}{\left(p_2 z_4^3 + q_2 z_4^2 + o_2 z_4 + \gamma_2\right)^2}}{\sum_{i=1,4} \dfrac{e_i}{\left(p_i z_i^3 + q_i z_i^2 + o_i z_i + \gamma_i\right)^2}}$$
$$\left. \times \left[\left(a_1' z_4 e^{b_1' z_4^{1.1}} - c_1' e^{d_1' z_4}\right) - C_2 \times \tanh(K z_5)\right]\right] \tag{16}$$

$$\dot{z}_6 = \frac{(V_2 - R_2 z_6)\left(C_{12} + C_{22}(g_{m2} - r_2 z_4)\right)}{N_2^2}$$
$$- \frac{r_2 C_{22} z_5 z_6}{\left(C_{12} + C_{22}(g_{m2} - r_2 z_4)\right)} \tag{17}$$

where b_{di} indicates the equivalent torsional damping, k_i is the equivalent torsional stiffness, V_i stands for the supply voltage, r_i indicates the radius of the pinion, C_1 and C_2 are the reluctances of the magnetic path without air gap and that of the air gap, respectively, N_i stands for the number of coils, g_{mi} is the nominal air gap, J_i indicates the polar moment of inertia of the valve's disk, and R_i is the electrical resistance of coil. $z_1 = \alpha_1$, $z_2 = \dot{\alpha}_1$, and $z_3 = i_1$ indicate the upstream valve's rotation angle, angular velocity, and actuator current, respectively. $z_4 = \alpha_2$, $z_5 = \dot{\alpha}_2$, and $z_6 = i_2$ stand for the downstream valve's rotation angle, angular velocity, and actuator current, respectively. The network parameters are listed in Table 1.

Note that we could capture, for the first time, the coupled chaotic and hyperchaotic dynamics of the interconnected sets [1] by examining the critical values of $b_{di} = \mu_i = 1 \times 10^{-7}$ for two different initial conditions of $\text{Initial}_1 = [20(\text{deg})\,0\,0\,20(\text{deg})\,0\,0]$ and $\text{Initial}_2 = [2(\text{deg})\,0\,0\,2(\text{deg})\,0\,0]$, respectively. Shown in Figs. 2(*a*) and 2(*b*) are the chaotic and hyperchaotic dynamics of the

Table 1 The system parameters

ρ	$1000\,(\text{kg/m}^3)$	v	3 m/s
$J_{1,2}$	$0.104 \times 10^{-1}\,\text{kg m}^2$	N_2	3300
N_1	3300	$C_{11,22}$	$1.56 \times 10^6 (H^{-1})$
D_{v1}	0.2032 m	D_{v2}	0.127 m
$D_{s1,s2}$	0.01 m	P_{out}	2 kPa
$k_{1,2}$	$60\,\text{N·m}^{-1}$	$C_{21,22}$	$6.32 \times 10^8 (H^{-1})$
L_1	2 m	L_2	1 m
$r_{1,2}$	0.05 m	θ	90 deg
P_{in}	256 kPa	$g_{m1,m2}$	0.1 m
μ_f	$0.018\,\text{kg m}^{-1}\,\text{s}^{-1}$	$\lambda_{1,2}$	1
$n_{1,2}$	10	$b_{di} = \mu_i$	1×10^{-7}

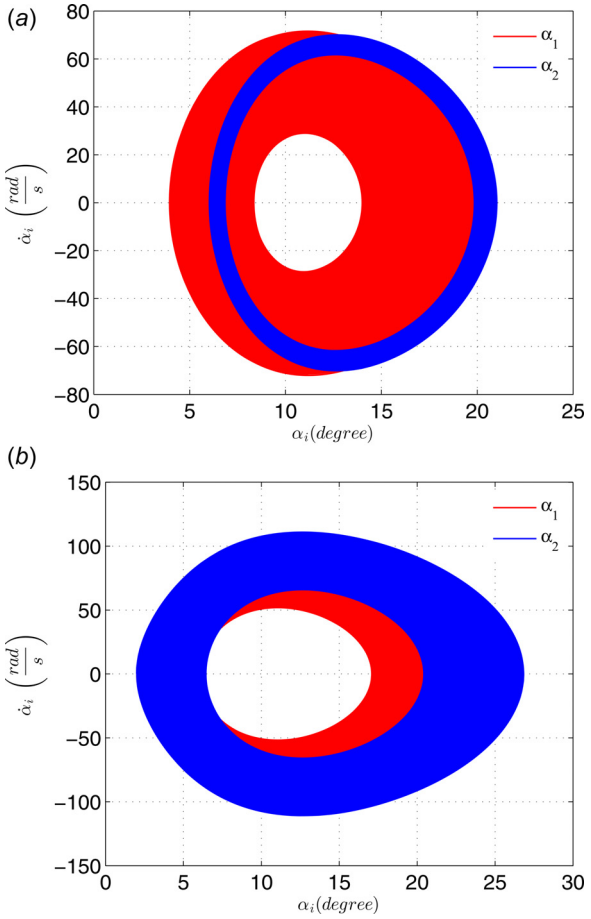

Fig. 2 (*a*) The coupled sets' phase portraits for Initial_1 and (*b*) the coupled sets' phase portraits for Initial_2

coupled actuated valves, respectively; the red and blue lines indicate the angular velocities versus rotation angles of the upstream and downstream valves, respectively. Some powerful tools of the nonlinear analysis, including the Lyapunov exponents and Poincaré map [32], were used in distinguishing among the nature of harmful responses, as shown in Figs. 3(*a*)–3(*f*). One and two positive Lyapunov exponents along with irregular Poincaré maps confirmed the chaotic and hyperchaotic dynamics of the actuated valves, respectively. Such dangerous responses need to be vanished using a nonlinear control scheme, due to the nonlinear and coupled nature of the network, in order to return the interconnected sets to their stable domains. The operationally optimized valves' motions, on the other hand, are utilized in the nonlinear control scheme as desirable trajectories. Based on the inevitable unknown parameters of such a coupled network, the nonlinear model-based adaptive scheme looks as an effective approach to be employed in stabilizing the system subject to the chaotic and hyperchaotic dynamics.

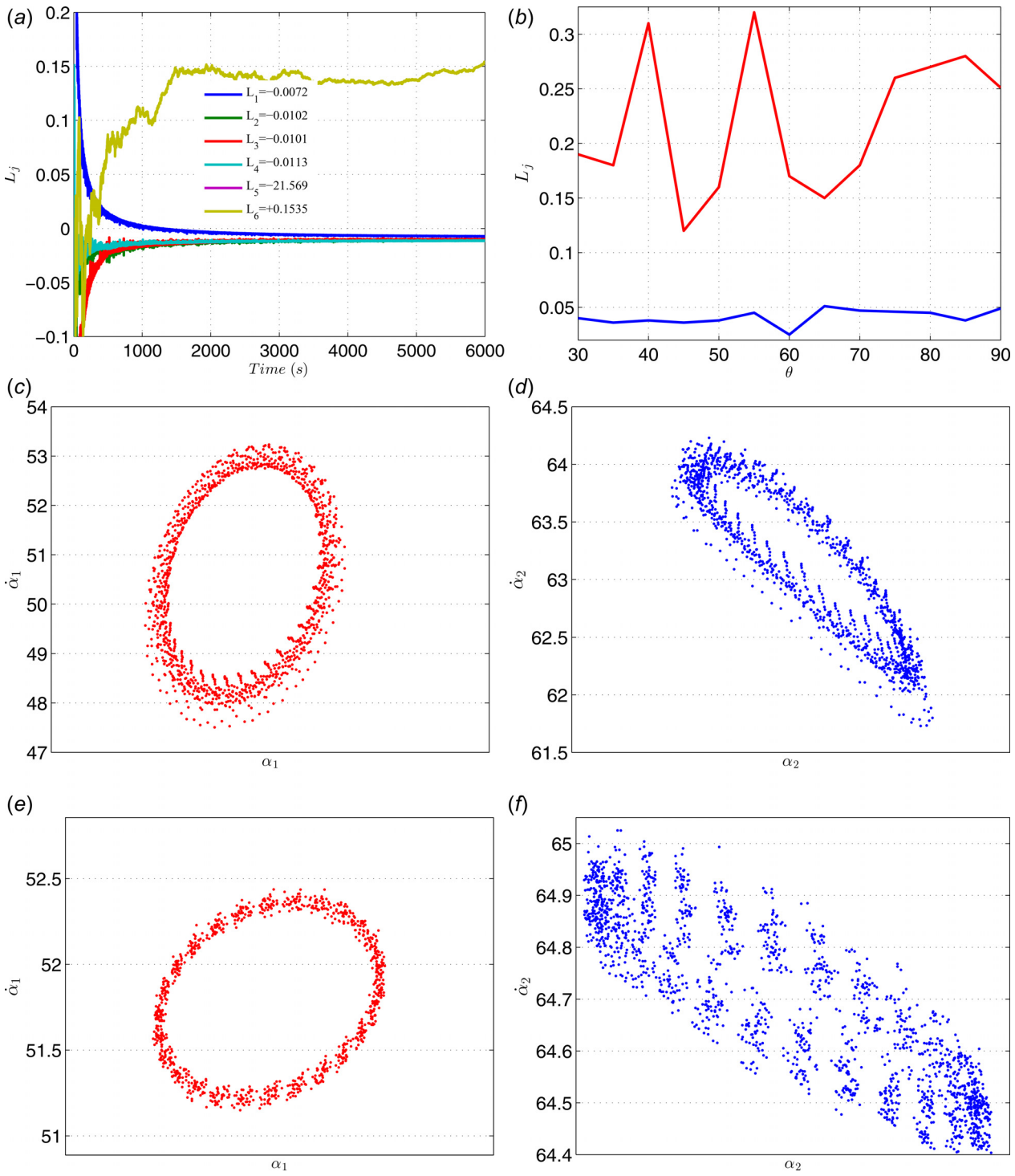

Fig. 3 (*a*) The Lyapunov exponents for Initial$_1$, (*b*) the positive Lyapunov exponents for Initial$_2$ versus different approach angles (θ), (*c*) the Poincaré map for Initial$_1$ of the upstream set, (*d*) the Poincaré map for Initial$_1$ of the downstream set, (*e*) the Poincaré map for Initial$_2$ of the upstream set, and (*f*) the Poincaré map for Initial$_2$ of the downstream set

3 Control and Adaptation Laws

The nonlinear model-based adaptive control method [33–35] is used in stabilizing the unstable system in order to track the desired trajectories [1,3] defined based on the critical initial conditions as follows:

$$\alpha_{di} = \frac{\pi}{3}\tanh(10^{-4}t^3) + \frac{\pi}{9}, \quad \text{Initial}_1 \tag{18}$$

$$\alpha_{di} = \frac{\pi}{3}\tanh(10^{-4}t^3) + \frac{\pi}{90}, \quad \text{Initial}_2 \tag{19}$$

The so-called "S-Shaped" trajectories are highly energy-efficient [3] and yield smooth dynamic responses avoiding the repeatedly observed dangerous phenomenon of "Water Hammering." The coupled dynamic Eqs. (13) and (16) can be rewritten as the following:

$$J_1\ddot{\alpha}_1 + b_{d1}\dot{\alpha}_1 + k_1\alpha_1 = \frac{r_1 C_{21} N_1^2 i_1^2}{2\left(C_{11} + C_{21}(g_{m1} - r_1\alpha_1)\right)^2} + \frac{A_1 R_{n1}}{\sum_{i=1}^{2} R_{ni}}\left[T'_{h1} - T'_{b1}\tanh(K\dot{\alpha}_1)\right] \tag{20}$$

$$J_2\ddot{\alpha}_2 + b_{d2}\dot{\alpha}_2 + k_2\alpha_2 = \frac{r_2 C_{22} N_2^2 i_2^2}{2\left(C_{21} + C_{22}(g_{m2} - r_2\alpha_2)\right)^2} + \frac{A_1 R_{n2}}{\sum_{i=1}^{2} R_{ni}}\left[T'_{h2} - T'_{b2}\tanh(K\dot{\alpha}_2)\right] \tag{21}$$

where $A_1 = (P_{\text{in}} - P_{\text{out}} - (R_{L1} + R_{L2} + R_{\text{con}}q_v)q_v)$, $T'_{h1} = a_1\alpha_1 e^{b_1\alpha_1{}^{1.1}} - c_1 e^{d_1\alpha_1}$, $T'_{h2} = a'_1\alpha_2 e^{b'_1\alpha_2^{1.1}} - c'_1 e^{d'_1\alpha_2}$, $T'_{b1} = C_1$, and $T'_{b2} = C_2$. Assuming

$$M_1 = \frac{2J_1\left(C_{11} + C_{21}(g_{m1} - r_1\alpha_1)\right)^2}{r_1 C_{21} N_1^2},$$

$$M_2 = \frac{2J_2\left(C_{21} + C_{22}(g_{m2} - r_2\alpha_2)\right)^2}{r_2 C_{22} N_2^2}$$

$$B_1 = \frac{2b_{d1}\left(C_{11} + C_{21}(g_{m1} - r_1\alpha_1)\right)^2}{r_1 C_{21} N_1^2},$$

$$B_2 = \frac{2b_{d2}\left(C_{21} + C_{22}(g_{m2} - r_2\alpha_2)\right)^2}{r_2 C_{22} N_2^2}$$

$$K_1 = \frac{2k_1\left(C_{11} + C_{21}(g_{m1} - r_1\alpha_1)\right)^2}{r_1 C_{21} N_1^2},$$

$$K_2 = \frac{2k_2\left(C_{21} + C_{22}(g_{m2} - r_2\alpha_2)\right)^2}{r_2 C_{22} N_2^2}$$

$$Co_1 = \frac{2\left(C_{11} + C_{21}(g_{m1} - r_1\alpha_1)\right)^2}{r_1 C_{21} N_1^2},$$

$$Co_2 = \frac{2\left(C_{21} + C_{22}(g_{m2} - r_2\alpha_2)\right)^2}{r_2 C_{22} N_2^2}$$

Equations (20) and (21) can be rewritten as follows:

$$M_1\ddot{\alpha}_1 + B_1\dot{\alpha}_1 + K_1\alpha_1 = u_1 + \frac{A_1 Co_1 R_{n1}}{\sum_{i=1}^{2} R_{ni}}\left[T'_{h1} - T'_{b1}\tanh(K\dot{\alpha}_1)\right] \tag{22}$$

$$M_2\ddot{\alpha}_2 + B_2\dot{\alpha}_2 + K_2\alpha_2 = u_2 + \frac{A_1 Co_2 R_{n2}}{\sum_{i=1}^{2} R_{ni}}\left[T'_{h2} - T'_{b2}\tanh(K\dot{\alpha}_2)\right] \tag{23}$$

We define the valves' tracking errors and their first- and second-time derivatives as the following:

$$e_i = \alpha_{di} - \alpha_i, \quad \dot{e}_i = \dot{\alpha}_{di} - \dot{\alpha}_i, \quad \ddot{e}_i = \ddot{\alpha}_{di} - \ddot{\alpha}_i, \quad (i = 1, 2)$$

This yields

$$M_1\ddot{e}_1 = M_1\ddot{\alpha}_{d1} - M_1\ddot{\alpha}_1 = M_1\ddot{\alpha}_{d1} + B_1\dot{\alpha}_1 + K_1\alpha_1 - u_1 - \frac{A_1 Co_1 R_{n1}}{\sum_{i=1}^{2} R_{ni}}\left[T'_{h1} - T'_{b1}\tanh(K\dot{\alpha}_1)\right] \tag{24}$$

$$M_2\ddot{e}_2 = M_2\ddot{\alpha}_{d2} - M_2\ddot{\alpha}_2 = M_2\ddot{\alpha}_{d2} + B_2\dot{\alpha}_2 + K_2\alpha_2 - u_2 - \frac{A_1 Co_2 R_{n2}}{\sum_{i=1}^{2} R_{ni}}\left[T'_{h2} - T'_{b2}\tanh(K\dot{\alpha}_2)\right] \tag{25}$$

The combined tracking errors [33–35] and their first-time derivatives are as follows:

$$s_i = \dot{e}_i + \lambda_i e_i, \quad \dot{s}_i = \ddot{e}_i + \lambda_i \dot{e}_i, \quad (i = 1, 2)$$

where λ's are strictly positive numbers listed in Table 1. Premultiplying by M_1 and M_2 and substituting from Eqs. (24) and (25), we have

$$M_1\dot{s}_1 = M_1\ddot{\alpha}_{d1} + B_1\dot{\alpha}_1 + K_1\alpha_1 - u_1 - \frac{A_1 Co_1 R_{n1}}{\sum_{i=1}^{2} R_{ni}} \times \left[T'_{h1} - T'_{b1}\tanh(K\dot{\alpha}_1)\right] + M_1\lambda_1\dot{e}_1 \tag{26}$$

$$M_2\dot{s}_2 = M_2\ddot{\alpha}_{d2} + B_2\dot{\alpha}_2 + K_2\alpha_2 - u_2 - \frac{A_1 Co_2 R_{n2}}{\sum_{i=1}^{2} R_{ni}} \times \left[T'_{h2} - T'_{b2}\tanh(K\dot{\alpha}_2)\right] + M_2\lambda_2\dot{e}_2 \tag{27}$$

Based on the interconnected dynamics of the network, we chose the following quadratic Lyapunov function candidate:

$$V = \frac{1}{2}\left[\sum_{i=1}^{2}\left(s_i^T M_i s_i + \tilde{\Theta}_i^T \Gamma_i^{-1}\tilde{\Theta}_i\right)\right] \tag{28}$$

where Γ_i is a symmetric positive definite matrix and $\tilde{\Theta}_i$ is the system's lumped parameter estimation error ($\tilde{\Theta}_i = \Theta_i - \hat{\Theta}_i$). Differentiating the Lyapunov function (Eq. (28)) yields

$$\dot{V} = \sum_{i=1}^{2}\left(s_i^T M_i\dot{s}_i + \frac{1}{2}s_i^T\dot{M}_i s_i - \tilde{\Theta}_i^T\Gamma_i^{-1}\dot{\hat{\Theta}}_i\right) = \sum_{i=1}^{2}\left[s_i^T\left[M_i\ddot{\alpha}_{di} + B_i\dot{\alpha}_i + K_i\alpha_i - u_i - \frac{A_1 Co_i R_{ni}}{\sum R_{ni}} \times \left[T'_{hi} - T'_{bi}\tanh(K\dot{\alpha}_i)\right] + M_i\lambda_i\dot{e}_i + \frac{1}{2}\dot{M}_i s_i\right] - \tilde{\Theta}_i^T\Gamma_i^{-1}\dot{\hat{\Theta}}_i\right] \tag{29}$$

By defining the regression vectors as the following:

$$W_i\Theta_i = M_i\ddot{\alpha}_{di} + B_i\dot{\alpha}_i + K_i\alpha_i - \frac{A_1 Co_i R_{ni}}{\sum R_{ni}} \times \left[T'_{hi} - T'_{bi}\tanh(K\dot{\alpha}_i)\right] + M_i\lambda_i\dot{e}_i + \frac{1}{2}\dot{M}_i s_i, \ (i = 1, 2) \tag{30}$$

The $\dot{V}$ can be easily rewritten as follows:

$$\dot{V} = \sum_{i=1}^{2} [s_i^T [W_i \Theta_i - u_i] - \tilde{\Theta}_i^T \Gamma_i^{-1} \dot{\hat{\Theta}}_i] \tag{31}$$

The appropriate control inputs are hence chosen as the following:

$$u_i = W_i \hat{\Theta}_i + n_i s_i, \quad (i = 1, 2) \tag{32}$$

where

$$W_i \hat{\Theta}_i = \hat{M}_i \ddot{\alpha}_{di} + \hat{B}_i \dot{\alpha}_i + \hat{K}_i \alpha_i - \frac{A_1 \hat{C}o_i R_{ni}}{\sum R_{ni}} \times \left[T'_{hi} - T'_{bi} \tanh(K \dot{\alpha}_i)\right] + \hat{M}_i \lambda_i \dot{e}_i + \frac{1}{2} \dot{\hat{M}}_i s_i, \quad (i = 1, 2) \tag{33}$$

We can easily develop both the regression ($W_i \in \Re^{1\times 17}$) and estimated lumped parameter vectors ($\hat{\Theta}_i \in \Re^{17\times 1}$) as shown in the Appendix.

Substituting the control inputs into Eq. (31) gives

$$\begin{aligned} \dot{V} &= \sum_{i=1}^{2} s_i^T [\underbrace{W_i \Theta_i - W_i \hat{\Theta}_i}_{W_i \tilde{\Theta}_i} - n_i s_i] - \tilde{\Theta}_i^T \Gamma_i^{-1} \dot{\hat{\Theta}}_i \\ &= \sum_{i=1}^{2} s_i^T W_i \tilde{\Theta}_i - s_i^T n_i s_i - \tilde{\Theta}_i^T \Gamma_i^{-1} \dot{\hat{\Theta}}_i \\ &= \sum_{i=1}^{2} [s_i^T W_i - \Gamma_i^{-1} \dot{\hat{\Theta}}_i^T] \tilde{\Theta}_i - s_i^T n_i s_i \end{aligned} \tag{34}$$

which leads us to develop the following parameters' adaptation laws:

$$\dot{\hat{\Theta}}_i = \Gamma_i W_i^T s_i \tag{35}$$

Substituting Eq. (35) into Eq. (34) yields

$$\dot{V} = \sum_{i=1}^{2} -s_i^T n_i s_i \leq 0 \tag{36}$$

Based on Eq. (36), we need to prove $\dot{V} \to 0$ as $t \to \infty$ revealing $s_i \to 0$ as $t \to \infty$, or simply

$$\{\dot{V} \to 0 \Rightarrow s_i \to 0\}$$

Since V is positive, Barbalat's lemma [33–35] confirms that $\dot{V}$ approaches zero if it is uniformly continuous and its time derivative $\ddot{V}$ is bounded

$$\{\ddot{V} \text{ is bounded} \Rightarrow \dot{V} \to 0 \Rightarrow s_i \to 0\}$$

We can easily derive $\ddot{V}$ as follows:

$$\ddot{V} = -2 \sum_{i=1}^{2} s_i^T n_i \dot{s}_i \tag{37}$$

Equation (37) implies

$$\{s_i \text{ and } \dot{s}_i \text{ are bounded} \Rightarrow \ddot{V} \text{ is bounded} \Rightarrow \dot{V} \to 0 \Rightarrow s_i \to 0\}$$

Note that V is bounded due to $V \geq 0$ and $\dot{V} \leq 0$ indicating that s_i and $\tilde{\Theta}_i$ are also bounded. This would, in turn, reveals that α_i, $\dot{\alpha}_i$, α_{di}, $\dot{\alpha}_{di}$, $\ddot{\alpha}_{di}$ ($s_i = f(\alpha_i, \dot{\alpha}_i, \dot{\alpha}_{di}, \alpha_{di})$) and $\hat{\Theta}_i$ are bounded. Combining Eqs. (26), (27), (30), and (32) gives

$$M_i \dot{s}_i + \left[n_i + \frac{1}{2} \dot{M}_i\right] s_i = W_i \tilde{\Theta}_i, \quad (i = 1, 2) \tag{38}$$

Note that the bounded α_i and $\dot{\alpha}_i$ result in bounded M_i and $\dot{M}_i$ yielding bounded $\dot{s}_i$ due to the bounded s_i, W_i, and $\tilde{\Theta}_i$. The bounded s_i and $\dot{s}_i$ result in the bounded $\ddot{V}$ and one can easily conclude that $\dot{V}$ and $s_i \to 0$ as $t \to \infty$ [33–35]. This obviously indicates that e_i and $\dot{e}_i$ tend to zero as $t \to \infty$.

We, hence, guarantee both the global stability of the coupled network (the boundedness of α_i, $\dot{\alpha}_i$, and $\hat{\Theta}_i$) and convergence of the tracking errors (e_i). We have implemented the formulations, and adaptation and control laws in MATLAB and captured interesting results.

4 Results

The values of n_i used in the coupled control inputs (Eq. (32)) are listed in Table 1 and $\Gamma_i = \text{diag}[10]_{17\times 17}$. Figures 4 and 5 present the estimation process of the unknown parameters (Θ_1–Θ_{34}) for both the upstream and downstream sets subject to the Initial$_1$

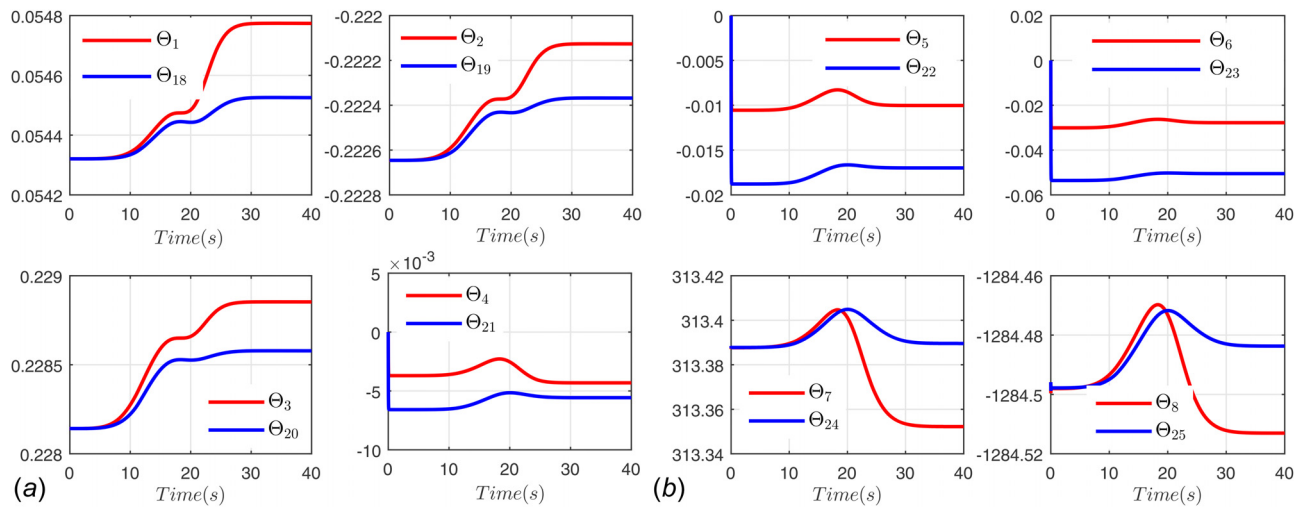

Fig. 4 The parameter estimation for Θ_1–Θ_8 of the upstream set and Θ_{18}–Θ_{25} of the downstream set

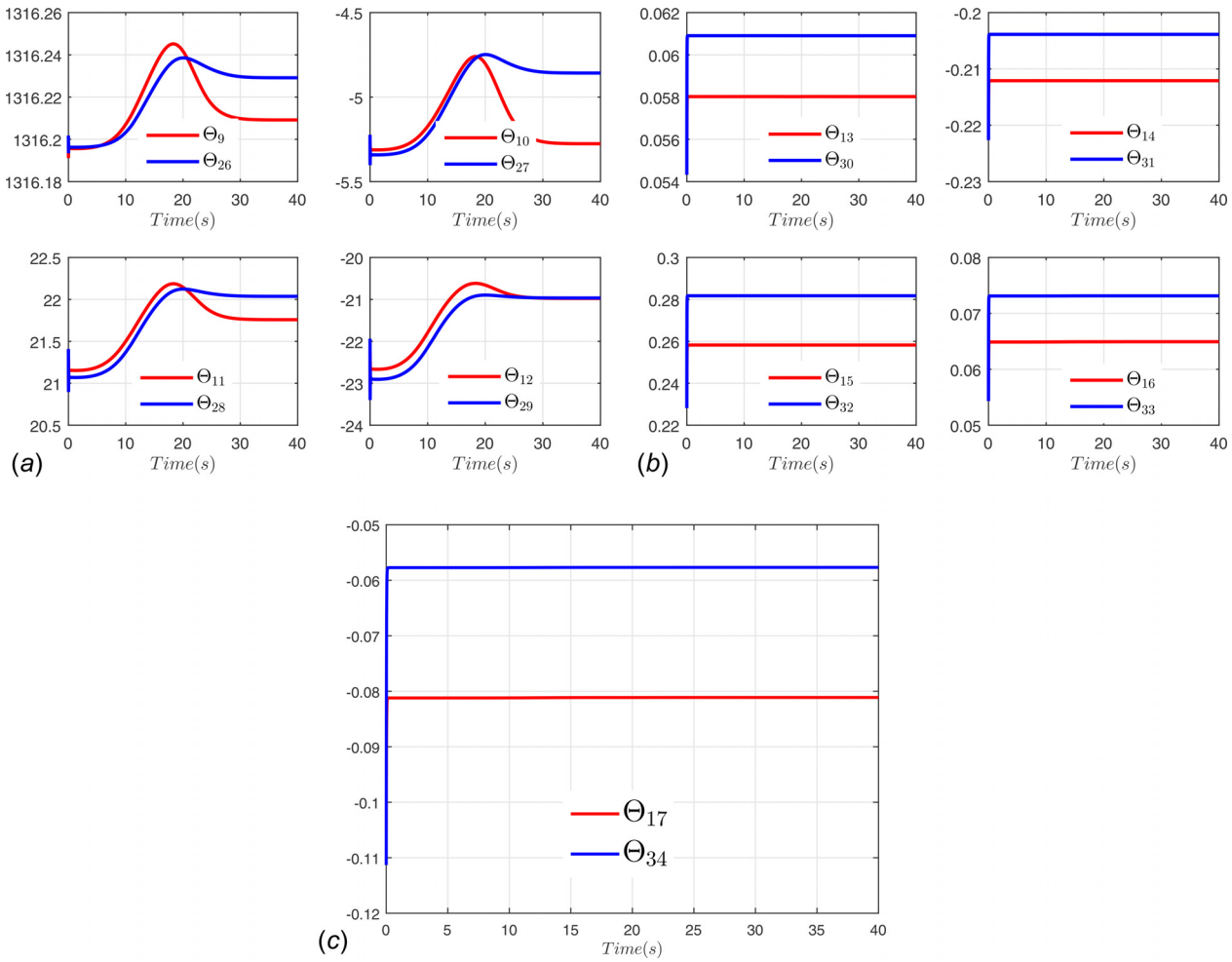

Fig. 5 The parameter estimation for Θ_9–Θ_{17} of the upstream set and Θ_{26}–Θ_{34} of the downstream set

revealing the parameters convergence within the nominal operation time of 40 s; the Initial$_1$ yielded the coupled chaotic dynamics. The Θ_1–Θ_{17} and Θ_{18}–Θ_{34} indicate the parameters of the upstream and downstream sets, respectively. Note that the initial values of Θ_1–Θ_{34} used in the adaptation laws are 90% of their nominal values we developed through the Appendix. Such initial values are intentionally selected to yield meaningful estimated parameters with respect to the electro-magneto-mechanical-fluid nature of the network. It is of a great interest to observe that, despite the dominant chaotic dynamics resulted from the Initial$_1$, the parameters timely converge, and therefore, we expect to observe stable operations of both the coupled actuated valves. Note that this approach, based on the "sufficient richness" condition [33–35], would not exactly estimate the unknown parameters such that it expectedly yields values to allow the desired task to be carried out.

The estimated parameters, based on Eq. (32), would help generate powerful control inputs, the applied currents of the bi-directional solenoid actuators (i_i), to vanish the chaotic dynamics of the interconnected sets (Fig. 2(*a*)) and then drive the coupled valves to track the desirable trajectories, which we addressed earlier (Eq. (18)). Shown in Fig. 6(*a*) are the control inputs for both the upstream and downstream actuators. As expected, the currents consist of two phases as shown in Fig. 6(*a*). The first phase, with oscillatory negative values of the currents, suppresses the coupled chaotic dynamics due to the Initial$_1$ resulting in downward/slightly upward motions of the plungers, which would consequently avoid the sudden jumps of the valves. During the second phase of the control process, the currents gradually take positive values indicating that the plungers move upward, and therefore, the valves rotate toward the desirable trajectories.

It is of a great interest to observe that the control input of the downstream set is remarkably higher than that of the upstream one, in particular for the first phase of the control process. The physical interpretation of such higher values of the control input used in the downstream set can be explained through the effects of the flow loads acting on the valve, in particular the hydrodynamic torque

$$\frac{T_{h2}}{T_{h1}} \propto \left(\frac{D_{v2}}{D_{v1}}\right)^3 \times \left(\frac{c_{v1}}{c_{v2}}\right)^2 \tag{39}$$

$$\frac{T_{b2}}{T_{b1}} \propto \left(\frac{D_{v2}c_{v1}}{D_{v1}c_{v2}}\right)^2 \tag{40}$$

where c_{v1} and c_{v2} are the upstream and downstream valves' coefficients, respectively, $(c_{vi}(\alpha_i) = p_i\alpha_i^3 + q_i\alpha_i^2 + o_i\alpha_i + \gamma_i)$; we have provided the values of p_i, q_i, o_i, and γ_i in Sec. 2. We have previously reported [1–3,9,10,12] that a smaller pipe diameter yields both the higher hydrodynamic and bearing torques due to the higher coefficient of the upstream valve than that of the downstream one (Eqs. (39) and (40)). From another aspect, the hydrodynamic torque is a helping load [1–6,8–13] to close the symmetric valve whereas the bearing one is a resistance (friction-based) torque for the valve's operation. The downstream set with a smaller pipe diameter, subject to the chaotic dynamics of the Initial$_1$, undoubtedly needs more suppressing control input to

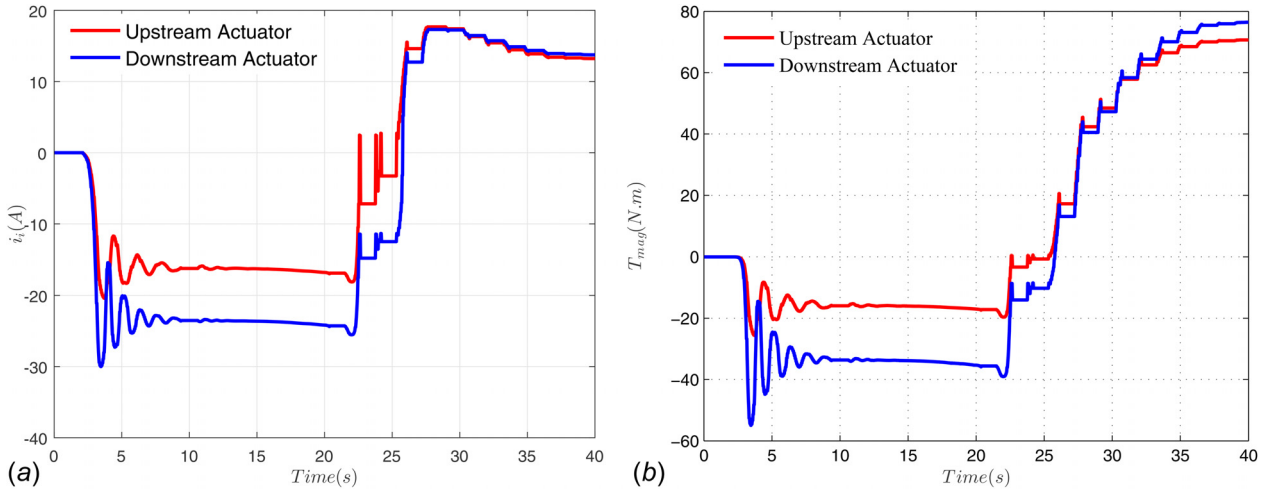

Fig. 6 (*a*) The control inputs and (*b*) the magnetic torques

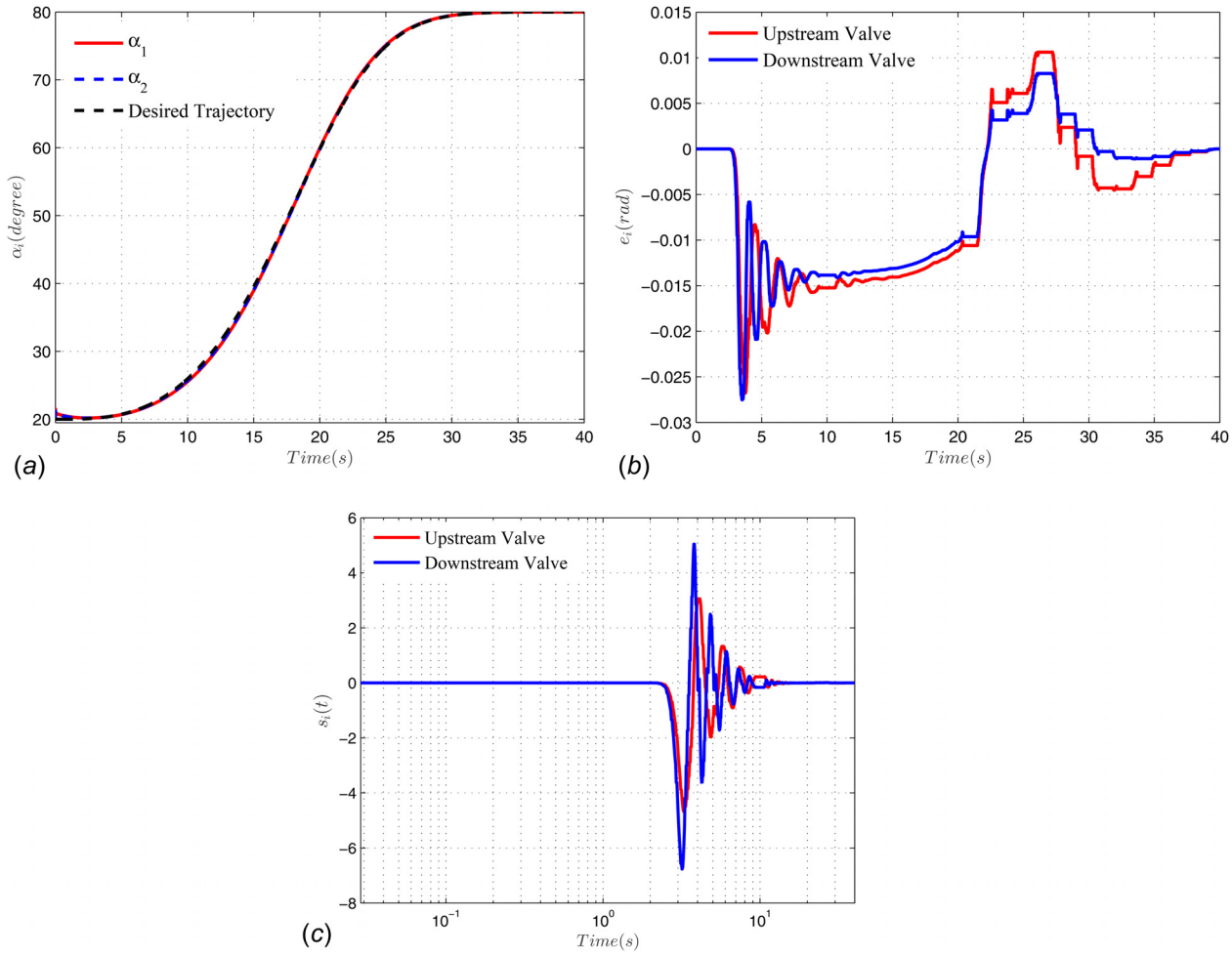

Fig. 7 (*a*) The valves' rotation angles, (*b*) the error signals, and (*c*) the combined tracking error signals

mitigate the destabilizer effects of the higher hydrodynamic torque acting on the valve. For the second phase of the control process, the higher resistance bearing torque acting on the downstream set inevitably demands slightly higher control input to push the valve to the desirable trajectory.

Such profiles of the control inputs for both the sets are expected to be observed for the driving magnetic torques (forces) as nonlinear functions of the control inputs in addition to the valves' rotation angles/plungers' displacements. Figure 6(*b*) presents the driving magnetic torques of both the coupled sets in which the two phases of the control process can be distinguished as we discussed for the currents. The oscillatory negative values of the magnetic torques suppress the chaotic dynamics along with mitigating the effects of the hydrodynamic torques. The positive

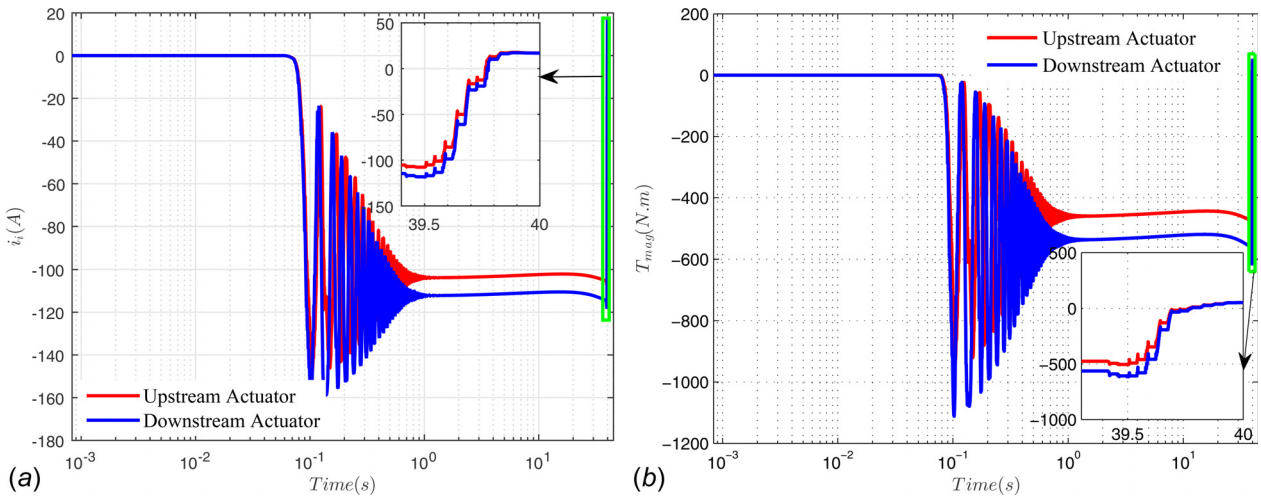

Fig. 8 (*a*) The control inputs and (*b*) the magnetic torques

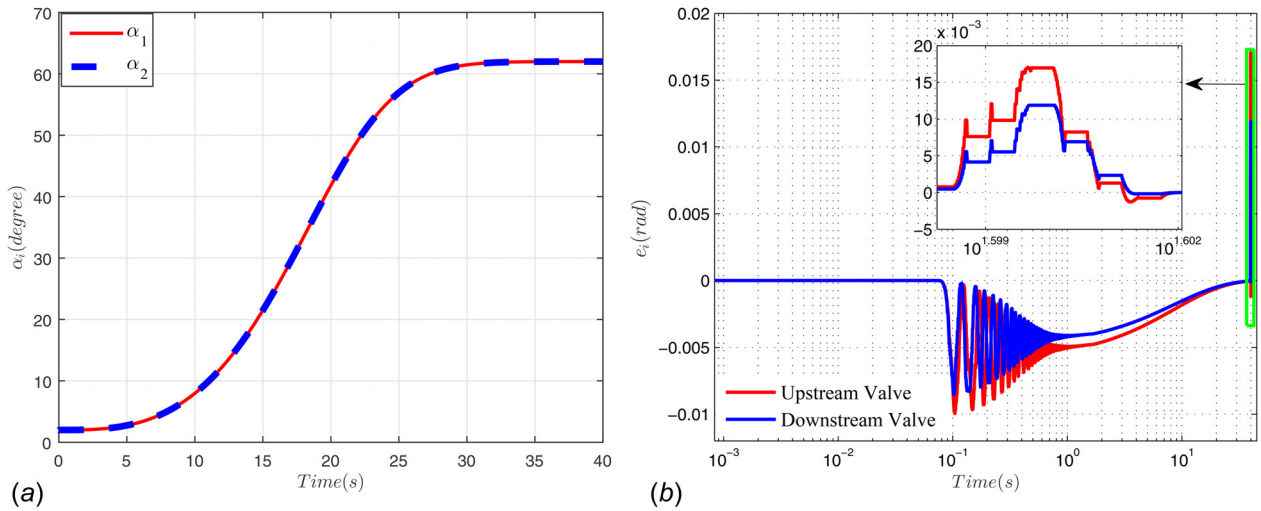

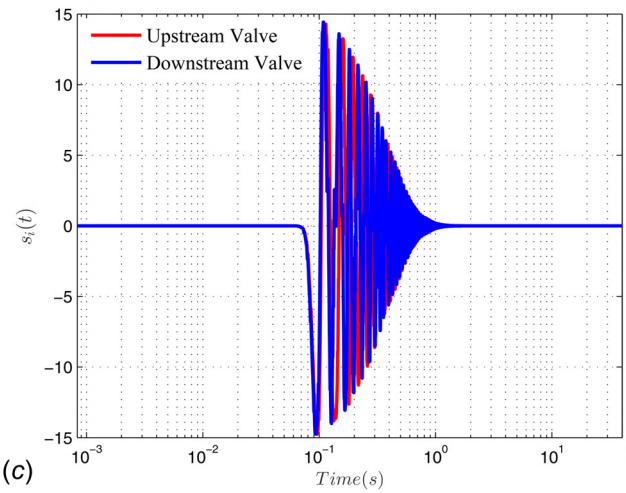

Fig. 9 (*a*) The valves' rotation angles, (*b*) the error signals, and (*c*) the combined tracking error signals

magnetic torques (forces) move the plungers upward and subsequently, the valves move toward the desirable trajectories. The higher amount of the driving magnetic torque of the downstream set, for the second phase of the control process, looks logical to overcome the higher resistance bearing torque than that of the upstream one.

Shown in Fig. 7(*a*) are the upstream and downstream valves' rotation angles indicating that both the sets track the desirable

trajectories (Eq. (18)) by applying the control inputs which expectedly vanish the coupled chaotic dynamics due to the Initial$_1$. Both the error (e_i) and combined tracking error (s_i) signals shown in Figs. 7(*b*) and 7(*c*), respectively, converge to zero revealing that the valves' angles (α_i) tend to the desirable trajectories (α_{di}) within the nominal operation time.

Figures 8(*a*) and 8(*b*) present the control inputs and driving magnetic torques, respectively, used in vanishing the coupled hyperchaotic dynamics caused by the Initial$_2$ (Fig. 2(*b*)). As expected, the hyperchaotic dynamics of both the sets with the larger domains of attractions, which we have thoroughly addressed in Refs. [1] and [3], would require significantly higher values of the control inputs to be vanished than those of the chaotic ones. The considerable control inputs expectedly result in the higher driving magnetic torques than the ones used in the network subject to the chaotic dynamics (Fig. 8(*b*)). The two phases of the control process, which we discussed for the chaotic case, can be observed for the hyperchaotic one such that the oscillatory negative control inputs/driving magnetic torques suppress the hyperchaotic dynamics. Note that the boxes shown in Figs. 8(*a*) and 8(*b*) reveal the incremental values of the control inputs/torques to rotate the valves to the desirable trajectories.

Shown in Fig. 9(*a*) are both the upstream and downstream valves' rotation angles revealing that the valves' motions tend to the desirable trajectories (Eq. (19)). Figures 9(*b*) and 9(*c*) present the convergence of both the error and combined tracking error signals to zero, respectively. Consequently, it is straightforward to conclude that the adaptation and control laws guarantee both the global stability of the coupled network and convergence of the tracking errors in which we analytically discussed in Sec. 3.

5 Conclusions and Future Work

In this paper, we represented the interconnected sixth-order dynamic model of the network of two bi-directional solenoid actuated butterfly valves subject to the sudden contraction. The network undergoes the coupled chaotic and hyperchaotic dynamics for a set of initial conditions, the Initial$_1$ and Initial$_2$, and critical parameters. The adaptation and control laws were developed to vanish the chaotic/hyperchaotic dynamics and then push the dynamically coupled valves to track the desirable trajectories.

For the initial conditions resulted in the chaotic/hyperchaotic dynamics, we revealed that the downstream set required the higher control inputs/driving magnetic torques than those of the upstream one. The two phases of the control process were also distinguished to vanish the chaotic/hyperchaotic dynamics in addition to mitigating the harmful effects of the hydrodynamic torque (as a helping load) which expectedly magnifies the amplitude of dangerous stochastic oscillation. The first phase by presenting the oscillatory negative control inputs removed the chaotic/hyperchaotic dynamics. The control inputs of the second phase gradually took the positive values to push the valves to the desirable trajectories. The control inputs of the downstream set were shown to be higher than those of the upstream one, for the second phase of both the chaotic and hyperchaotic cases, in order to overcome the higher resistance bearing torque. We have previously established that the bearing torque of the downstream set with a smaller pipe diameter is higher than that of the upstream one.

For the next step, a scalable interconnected dynamic model will be developed to be used in control of the large-scale networks. Although adding more agents would potentially increase computational burden, and therefore, combinatorial computationally efficient centralized schemes would be needed to control the network in the presence of coupled harmful responses. We would develop and examine such feasible and computationally efficient control strategies.

Appendix

$$W_i = \Bigg[\alpha_i^2\ddot{\alpha}_{di}, \alpha_i\ddot{\alpha}_{di}, \ddot{\alpha}_{di}, \alpha_i^2\dot{\alpha}_i, \alpha_i\dot{\alpha}_i, \dot{\alpha}_i, \alpha_i^3, \alpha_i^2, \alpha_i,$$

$$\times\frac{A_1R_{ni}}{\sum R_{ni}}\left[T'_{hi}-T'_{bi}\tanh(K\dot{\alpha}_i)\right]\alpha_i^2, \frac{A_1R_{ni}}{\sum R_{ni}}\left[T'_{hi}-T'_{bi}\tanh(K\dot{\alpha}_i)\right]\alpha_i,$$

$$\times\frac{A_1R_{ni}}{\sum R_{ni}}\left[T'_{hi}-T'_{bi}\tanh(K\dot{\alpha}_i)\right], \alpha_i^2\dot{e}_i, \alpha_i\dot{e}_i, \dot{e}_i, \alpha_i s_i, s_i\Bigg]$$

$$\hat{\Theta}_i = \Bigg[\frac{2\hat{J}_i\hat{r}_i\hat{C}_{2i}}{\hat{N}_i^2}, \frac{-4\hat{J}_i\left[\hat{C}_{2i}\hat{g}_{mi}+\hat{C}_{1i}\right]}{\hat{N}_i^2}, \frac{2\hat{J}_i\left[\hat{C}_{2i}\hat{g}_{mi}+\hat{C}_{1i}\right]^2}{\hat{N}_i^2\hat{r}_i\hat{C}_{2i}},$$

$$\times\frac{2\hat{b}_{di}\hat{r}_i\hat{C}_{2i}}{\hat{N}_i^2}, \frac{-4\hat{b}_{di}\left[\hat{C}_{2i}\hat{g}_{mi}+\hat{C}_{1i}\right]}{\hat{N}_i^2}, \frac{2\hat{b}_{di}\left[\hat{C}_{2i}\hat{g}_{mi}+\hat{C}_{1i}\right]^2}{\hat{N}_i^2\hat{r}_i\hat{C}_{2i}},$$

$$\times\frac{2\hat{k}_i\hat{r}_i\hat{C}_{2i}}{\hat{N}_i^2}, \frac{-4\hat{k}_i\left[\hat{C}_{2i}\hat{g}_{mi}+\hat{C}_{1i}\right]}{\hat{N}_i^2}, \frac{2\hat{k}_i\left[\hat{C}_{2i}\hat{g}_{mi}+\hat{C}_{1i}\right]^2}{\hat{N}_i^2\hat{r}_i\hat{C}_{2i}},$$

$$\times\frac{-2\hat{r}_i\hat{C}_{2i}}{\hat{N}_i^2}, \frac{4\left[\hat{C}_{2i}\hat{g}_{mi}+\hat{C}_{1i}\right]}{\hat{N}_i^2}, \frac{-2\left[\hat{C}_{2i}\hat{g}_{mi}+\hat{C}_{1i}\right]^2}{\hat{N}_i^2\hat{r}_i\hat{C}_{2i}},$$

$$\times\frac{2\lambda_i\hat{J}_i\hat{r}_i\hat{C}_{2i}}{\hat{N}_i^2}, \frac{-4\lambda_i\hat{J}_i\left[\hat{C}_{2i}\hat{g}_{mi}+\hat{C}_{1i}\right]}{\hat{N}_i^2}, \frac{2\lambda_i\hat{J}_i\left[\hat{C}_{2i}\hat{g}_{mi}+\hat{C}_{1i}\right]^2}{\hat{N}_i^2\hat{r}_i\hat{C}_{2i}},$$

$$\times\frac{2\hat{J}_i\hat{r}_i\hat{C}_{2i}}{\hat{N}_i^2}, \frac{-2\hat{J}_i\left[\hat{C}_{2i}\hat{g}_{mi}+\hat{C}_{1i}\right]}{\hat{N}_i^2}\Bigg]^T, \quad (i=1,2)$$

References

[1] Naseradinmousavi, P., Segala, D. B., and Nataraj, C., 2016, "Chaotic and Hyperchaotic Dynamics of Smart Valves System Subject to a Sudden Contraction," ASME J. Comput. Nonlinear Dyn., **11**(5), p. 051025.

[2] Naseradinmousavi, P., Krstic, M., and Nataraj, C., 2016, "Design Optimization of Dynamically Coupled Actuated Butterfly Valves Subject to a Sudden Contraction," ASME J. Mech. Des., **138**(4), p. 041402.

[3] Naseradinmousavi, P., Machiani, S. G., Ayoubi, M. A., and Nataraj, C., 2017, "Coupled Operational Optimization of Smart Valve System Subject to Different Approach Angles of a Pipe Contraction," J. Struct. Multidiscip. Optim., **55**(3), pp. 1001–1015.

[4] Naseradinmousavi, P., 2015, "A Novel Nonlinear Modeling and Dynamic Analysis of Solenoid Actuated Butterfly Valves Coupled in Series," ASME J. Dyn. Syst. Meas. Control, **137**(1), p. 014505.

[5] Naseradinmousavi, P., and Nataraj, C., 2013, "Optimal Design of Solenoid Actuators Driving Butterfly Valves," ASME J. Mech. Des., **135**(9), p. 094501.

[6] Naseradinmousavi, P., and Nataraj, C., 2012, "Transient Chaos and Crisis Phenomena in Butterfly Valves Driven by Solenoid Actuators," J. Commun. Nonlinear Sci. Numer. Simul., **17**(11), pp. 4336–4345.

[7] Lee, D., Naseradinmousavi, P., and Nataraj, C., 2012, "Nonlinear Model-Based Adaptive Control of a Solenoid-Valve System," J. Control Sci. Eng., **2012**, p. 846458.

[8] Naseradinmousavi, P., and Nataraj, C., 2011, "Nonlinear Mathematical Modeling of Butterfly Valves Driven by Solenoid Actuators," J. Appl. Math. Modell., **35**(5), pp. 2324–2335.

[9] Naseradinmousavi, P., Krstic, M., Bagheri, M., and Nataraj, C., 2016, "Coupled Chaotic and Hyperchaotic Dynamics of Actuated Butterfly Valves Operating in Series," ASME Paper No. DSCC2016-9601.

[10] Naseradinmousavi, P., Bagheri, M., and Nataraj, C., 2016, "Coupled Operational Optimization of Smart Valve System Subject to Different Approach Angles of a Pipe Contraction," ASME Paper No. DSCC2016-9627.

[11] Naseradinmousavi, P., and Nataraj, C., 2015, "Design Optimization of Solenoid Actuated Butterfly Valves Dynamically Coupled in Series," ASME Paper No. DSCC2015-9605.

[12] Naseradinmousavi, P., 2015, "Optimal Design of Solenoid Actuated Butterfly Valves Dynamically Coupled in Series," ASME Paper No. IMECE2015-50094.

[13] Naseradinmousavi, P., and Nataraj, C., 2011, "A Chaotic Blue Sky Catastrophe of Butterfly Valves Driven by Solenoid Actuators," ASME Paper No. IMECE2011-62608.
[14] Chang-Jian, C.-W., 2014, "Gear Dynamics Analysis With Turbulent Journal Bearings Mounted Hybrid Squeeze Film Damper-Chaos and Active Control Analysis," ASME J. Comput. Nonlinear Dyn., **10**(1), p. 011011.
[15] Morel, C., Vlad, R., and Morel, J.-Y., 2008, "Anticontrol of Chaos Reduces Spectral Emissions," ASME J. Comput. Nonlinear Dyn., **3**(4), p. 041009.
[16] Chen, D., and Liu, W., 2016, "Chaotic Behavior and Its Control in a Fractional-Order Energy Demand-Supply System," ASME J. Comput. Nonlinear Dyn., **11**(6), p. 061010.
[17] Wang, B., Shi, K., Zhang, C., and Zhu, D., 2015, "Fuzzy Generalized Predictive Control for Nonlinear Brushless Direct Current Motor," ASME J. Comput. Nonlinear Dyn., **11**(4), p. 041004.
[18] Luo, R., and Zeng, Y., 2015, "The Control and Synchronization of a Class of Chaotic Systems With Output Variable and External Disturbance," ASME J. Comput. Nonlinear Dyn., **11**(5), p. 051011.
[19] Reddy, B. S., and Ghosal, A., 2015, "Asymptotic Stability and Chaotic Motions in Trajectory Following Feedback Controlled Robots," ASME J. Comput. Nonlinear Dyn., **11**(5), p. 051012.
[20] Khamsuwan, P., and Kuntanapreeda, S., 2016, "A Linear Matrix Inequality Approach to Output Feedback Control of Fractional-Order Unified Chaotic Systems With One Control Input," ASME J. Comput. Nonlinear Dyn., **11**(5), p. 051021.
[21] Merat, K., Chekan, J. A., Salarieh, H., and Alasty, A., 2014, "Control of Discrete Time Chaotic Systems Via Combination of Linear and Nonlinear Dynamic Programming," ASME J. Comput. Nonlinear Dyn., **10**(1), p. 011008.
[22] Tian, X., and Fei, S., 2015, "Adaptive Control for Fractional-Order Micro-Electro-Mechanical Resonator With Nonsymmetric Dead-Zone Input," ASME J. Comput. Nonlinear Dyn., **10**(6), p. 061022.
[23] Aghababa, M. P., and Hashtarkhani, B., 2015, "Synchronization of Unknown Uncertain Chaotic Systems Via Adaptive Control Method," ASME J. Comput. Nonlinear Dyn., **10**(5), p. 051004.
[24] Li, C., Su, K., and Wu, L., 2012, "Adaptive Sliding Mode Control for Synchronization of a Fractional-Order Chaotic System," ASME J. Comput. Nonlinear Dyn., **8**(3), p. 031005.
[25] Arefi, M. M., 2016, "Adaptive Robust Stabilization of Rossler System With Time-Varying Mismatched Parameters Via Scalar Input," ASME J. Comput. Nonlinear Dyn., **11**(4), p. 041024.
[26] Templeton, B. A., Cox, D. E., Kenny, S. P., Ahmadian, M., and Southward, S. C., 2010, "On Controlling an Uncertain System With Polynomial Chaos and H_2 Control Design," ASME J. Dyn. Syst. Meas. Control, **132**(6), p. 061304.
[27] Alasty, A., and Salarieh, H., 2007, "Identification and Control of Chaos Using Fuzzy Clustering and Sliding Mode Control in Unmodeled Affine Dynamical Systems," ASME J. Dyn. Syst. Meas. Control, **130**(1), p. 011004.
[28] Treesatayapun, C., and Uatrongjit, S., 2005, "Controlling Chaos by Hybrid System Based on FREN and Sliding Mode Control," ASME J. Dyn. Syst. Meas. Control, **128**(2), pp. 352–358.
[29] Naseradinmousavi, P., 2012, "Nonlinear Modeling, Dynamic Analysis, and Optimal Design and Operation of Electromechanical Valve Systems," Ph.D. thesis, Villanova University, Villanova, PA.
[30] Bennett, C. O., and Myers, J. E., 1962, *Momentum, Heat, and Mass Transfer*, McGraw-Hill, New York.
[31] Massey, B. S., and Ward-Smith, J., 1998, *Mechanics of Fluids*, 7th ed., CRC Press, Boca Raton, FL.
[32] Nayfeh, A. H., and Balachandran, B., 1995, *Applied Nonlinear Dynamics: Analytical, Computational, and Experimental Methods*, Wiley, Hoboken, NJ.
[33] Krstić, M., Kanellakopoulos, I., and Kokotović, P., 1995, *Nonlinear and Adaptive Control Design*, Wiley-Interscience, New York.
[34] Krstic, M., and Kokotovic, P. V., 1995, "Control Lyapunov Functions for Adaptive Nonlinear Stabilization," Syst. Control Lett., **26**(1), pp. 17–23.
[35] Slotine, J. J. E., and Li, W., 1991, *Applied Nonlinear Control*, Prentice Hall, Upper Saddle River, NJ.